Theoretical Investigation of the Lift and Drag Characteristics of Flexible Parawings at Subsonic Speeds

ROBERT L. BASS III*
E. I. DuPont, Company, Richmond, Va.

AND

JOHN J. BERTIN†
University of Texas at Austin, Austin, Texas

A theoretical analysis supplemented with an experimental program has been conducted to determine the lift and drag characteristics of NASA-type parawings. The results of the experimental program showed that the flowfield at a given spanwise station is nearly two-dimensional and that the aerodynamic characteristics of a parawing are similar to those of a conventional wing. As a consequence, it was concluded that the lifting-line theory for conventional wings should yield a suitable prediction for parawing aerodynamics even though the parawings have low aspect ratios. Thus, lifting-line theory was applied to several parawing configurations to determine the lift, induced drag, center of pressure, etc. The skin-friction drag was estimated so that the total drag as well as the lift-to-drag ratios could be calculated. Comparison of theory and experiment indicates that the lifting line theory provides an adequate estimate of parawing aerodynamics within the linear range of the lift curve. In addition, a technique based on the center of pressure results has been devised to predict the angle-of-attack at which trailing edge flutter begins.

Nomenclature

$\bar{A}_o$ = parawing flat-planform area
A_n = coefficients in circulation series
AR = aspect ratio, $b^2/\bar{A}_o$
b = wing span
Ch = actual chord
C_D = drag coefficient, $D/q_\infty \bar{A}_o$
C_{Di} = induced drag coefficient
C_{Do} = profile drag coefficient
C_{Dle} = leading edge drag coefficient
$C_{do_{l=0}}$ = local profile drag coefficient at zero lift
C_{do} = local profile drag coefficient
C_{dc} = cross flow drag coefficient
C_L = lift coefficient, $L/q_\infty \bar{A}_o$
C_lCh/S = loading function
$(C_lCh/S)'$ = loading function slope, per degree
C_R = root chord
C_l = local lift coefficient
D = drag force
d = leading edge diameter
L = lift force
$(L/D)_{\max}$ = maximum lift-to-drag ratio
l = length of trailing edge of planform of inflated paraglider
l_K = keel length
l_{le} = leading edge length
q_∞ = free stream dynamic pressure
S = parawing semispan
X_{le} = local coordinate of leading edge
X,Y,Z = coordinates defined in Fig. 2
X',Y' = coordinates defined in Fig. 2
X'',Y'' = coordinates defined in Fig. 2
$\bar{Y}$ = center of pressure on semispan
α = geometric angle of attack, Eq. (5) and (8)
α_a = angle of attack for any section relative to the root chord, Eq. (4)
α_{Ch} = angle of local chord with respect to root chord
α_{fl} = angle of attack where trailing edge flutter occurs
α_K = keel angle of attack
$\alpha_{l=0}$ = local angle of zero lift
Δ = maximum trailing edge ordinate
ϵ = semiapex angle of inflated parawing
θ = transformed coordinate in Prandtl lifting line theory
Λ = leading edge sweep angle of inflated parawing
Λ_o = leading edge sweep angle of flat-planform parawing
μ = defined by Eq. (7)

Received February 14, 1969; revision received July 22, 1969.
* Research Scientist.
† Assistant Professor, Department of Aerospace Engineering. Member AIAA.

Introduction

THE subsonic portion of space vehicle re-entry poses many problems such as those dealing with the actual landing of the vehicle. The paraglider (Fig. 1) is a device for decelerating the vehicle to impact speeds while providing steer capabilities. Since Rogallo's preliminary investigation[1] a multitude of experimental investigations have been conducted on a wide range of paragliders. These investigations[2–6] include a variety of subsonic static tests. The studies consider the effects of canopy shape, leading edge diameter, wing sweep, trailing edge bolt rope, and camber and twist on the aerodynamic and control characteristics of the paraglider. Studies of paragliders[7–9] have been made at supersonic speeds up to a Mach number of 6.6. Pressure distributions on three rigid wings simulating paragliders with varied canopy curvature and leading edge sweep have been obtained[10–12] for low subsonic, transonic, and supersonic speeds up to a Mach number of 4.65.

Polhamus and Naeseth[2] investigated the theoretical lift characteristics of paraglider aerodynamics by using rigid-wing theory. An approximate technique was developed based on the Pankhurst method[13] for camber effects and the Weissinger method[14] for angle of attack and twist effects. A conical geometry was assumed for each wing lobe and the aerodynamic twist estimated by a combined linear and quadratic distribution across the semispan.

An extensive investigation into the theoretical aerodynamics of flexible wings at low speeds is presented in a five part series.[15–19] In these reports a fairly complete aerodynamic theory is developed for one- and two-lobed slender triangular parawings. The theoretical development is based

on two-dimensional sail theory[20] where the aerodynamic shape and loading are directly related to each other in a first order fashion. In part V, engineering prediction methods were developed for NASA-type parawings (leading edges and root chord of equal length and large slackness ratios). Only correlation techniques and empirical results were used in developing satisfactory aerodynamic predictions. The theory for triangular parawings was used only as an aid in developing the correlation procedures for the NASA-type parawing as it was not applicable for this type of wing. A review of methods for predicting parawing aerodynamics has recently been published.[21,22] The methods devised in Refs. 15 and 16 for the low aspect ratio, low canopy slackness triangular parawings are reviewed. In addition, use is made of the lifting line techniques similar to those of Polhamus and Naeseth for an investigation of two-lobed parawings including a consideration of drag.

The purpose of the present investigation was to develop a suitable theoretical method to predict the subsonic lift and drag characteristics of general NASA-type parawings. This analytical effort was intended to provide correlations for experimental force measurements,[23] which included only lift and drag measurements. Several configurations were constructed and used in the experimental program to assist in establishing a theoretical model for the flow. The theoretical method was devised using rigid wing techniques and the results are compared with the experimental data for small-diameter leading-edge parawings. These methods predict wing lift and drag (both induced and profile) within the operating range of the wing. Lift curve slope, angle of zero lift, flutter boundary, spanwise load distributions, and maximum lift-to-drag ratio are predicted. Although it was not originally included in the scope of the effort, it is believed that the procedures could be extended to compute the pitching moment also.

Experimental Program

The models used in the experimental portion of this investigation were of the conical type illustrated in Fig. 1. The leading edges and keel of the model frame were constructed of $\frac{5}{16}$-in. drill rod, which resulted in a leading edge diameter that was 2.55% of its length. The frame was constructed such that all three of its members remain in the same plane. The two leading edges were free to rotate in a plane to allow variation of the sweep angle.

The basic canopy patterns are defined by their flat-planform leading edge sweep angle Λ_o. For the models with equal leading edge and keel lengths, the basic canopy shapes are 35°, 40°, and 45° and for those whose leading edges are 1.53 times the keel length, 35°, 45°, and 50°.

The tests were conducted in The Univ. of Texas subsonic wind tunnel which has a 22-in. × 36-in. open test section. Data included measurement of the aerodynamic forces of lift and drag within the linear lift range and visual observation of the flow indicated by tuft patterns on the model surface and canopy distortion.

For a complete discussion of the data obtained in the current program, the reader is referred to Ref. 23. However, the principal results are as follows.

1) For each model tested the maximum L/D occurred with the least canopy curvature.

2) Increasing the aspect ratio of conical paragliders gave only a small increase in lift-to-drag ratio.

3) Increasing the leading edge diameter of a basic paraglider model gave a slight increase in lift properties with a greater drag increase, thus, reducing the lift-to-drag ratio.

4) Larger wing sweep angles increase the angle of zero lift with a corresponding decrease in lift-curve slope.

5) Dynamic pressure affects the trailing edge flutter point at low dynamic pressures.

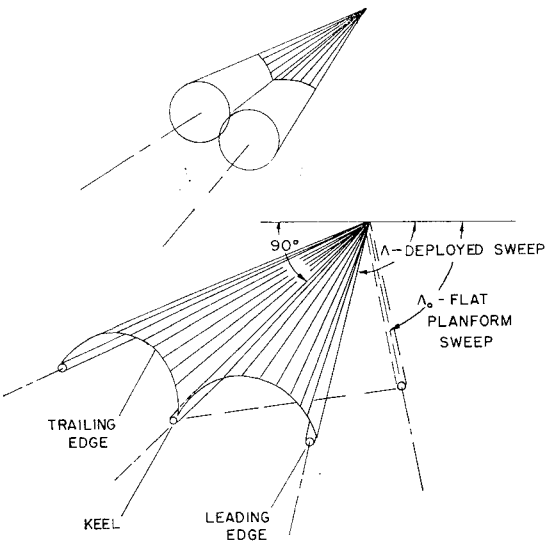

Fig. 1 Conical paragliders.

6) At low dynamic pressures paraglider canopies become distorted at low angles of attack in the region of canopy flutter with the slacker canopies remaining distorted the longest, but at high dynamic pressures the distortion and flutter occur almost simultaneously.

7) Tuft patterns indicate that flow is approximately two-dimensional within the range of linear wing lift.

Establishment of Analytical Model

Three types of experimental data were studied to determine a suitable method for predicting the lift and drag characteristics of parawings. The first type was lift and drag measurements from the literature and from an inhouse study, that were compared with the results for conventional wings. The second type was pressure data[10] in order to establish the trends in the pressure distribution on the parawing surface. The third type provided an understanding of the flowfield using tufts to study the parawing flow patterns. The results of these observations indicated that the application of finite wing theory should result in a suitable prediction of parawing lift and induced drag.

Since parawings of the NASA type can have large canopy slackness, they are unlike most conventional wings that are relatively flat except for small amounts of camber and twist. However, examination of the experimental lift curves for NASA parawings indicates that, as with conventional wings, they exhibit a linear rise in lift with angle of attack up to some point where the flow separates from the wing surface. The lift then decreases with angle of attack. The drag properties of these wings also compare favorably with conventional wings. Empirical relations[19] which are based on drag data[3] tend to substantiate this fact, i.e., parawing drag increases approximately as the square of the lift within the linear lift range of the wings.

The second approach was to examine pressure data[10] in which three rigid models simulating a 45° basic flat planform parawing with leading edge sweep angles of 48.6°, 52.5°, and 61.6° were constructed. Pressure data were obtained along the surface from the leading to the trailing edge at four positions of 0.2, 0.4, 0.6, and 0.8 of the semispan. Only pressures in the angle of attack range in which the wing lift was linear (as determined from Ref. 3) were examined. This range was approximately 15–35°, 18–40°, and 21–45° for the 48.6°, 52.5°, and 61.6° models, respectively.

An over-all review of these pressure data indicates that within the operating range of these parawings the chordwise pressure is approximately constant over a large percentage of the chord and at any angle of attack certain sections exhibit

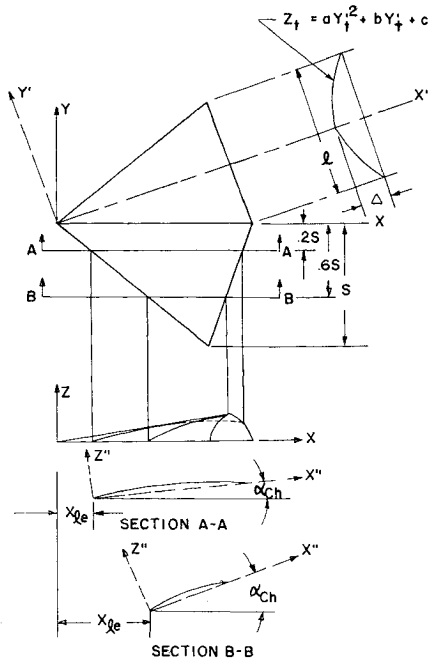

Fig. 2 Parawing coordinates.

this property more so than others. The spanwise pressure distributions are typical of wings with washout.

The third method employed was to observe the flow indicated by the tuft patterns on flexible models in the University of Texas subsonic wind tunnel. Tufts were attached to the surface of a $\Lambda_o = 45°$ NASA parawing model. Flow patterns were observed for various angles of attack for leading edge sweep angles of 50°, 60°, and 70° at a dynamic pressure of 5.0 psf. The tufts lined up well with the freestream for all three sweep angles at angles of attack near the flutter boundary, which corresponded to angles of attack of 14°, 22°, and 27° for sweep angles of 50°, 60°, and 70°, respectively. As the angle of attack was increased to the midrange of linear wing lift, the flow pattern near the nose and leading edge tended to turn outward but the tufts near the keel and trailing edge still remained aligned with the freestream. Also, the tufts attached to the leading edge did not exhibit any separation effects, indicating that the flow meets the canopy surface rather smoothly. For the 50° sweep angle, separation was observed at an angle of attack above the linear lift range which was an angle of attack of 34°. At this angle of attack, separation near the leading edges and over the majority of the canopy surface is evident from the tuft patterns. However, near the keel the tufts still remain aligned with the freestream.

The trailing edge tufts indicate that the flow was tangent to the canopy surface except near the wing tips at high angles of attack where the tufts began an oscillating motion. The tuft studies also indicate that the flow is approximately two-dimensional over the majority of the wing surface, while cross flow patterns typical of low aspect ratio, highly swept delta wings were not present. This two-dimensional flow pattern was most apparent between the two canopy lobes in the vicinity of the keel. It would appear from these studies that the shape of the canopy lobes tends to prevent the air from flowing from the leading edges toward the center of the wing. The result being that the flow is forced to move between the lobes and parallel to the keel near the center of the wings and is forced slightly outward in the vicinity of the leading edges.

The closest approximation to potential flow about a finite wing is obtained by using a distribution of vorticity over the wing surface. Since the application of surface theory is laborious and requires a large amount of computer time, one of the lifting-line theories is usually employed. The lifting-line approach proceeds on the assumptions that the flow about each unit span is two-dimensional and this is supported by the tuft study. Also, the tuft study upholds the Kutta condition at the trailing edge. The lifting line theory predicts a linear lift curve and the experimental evidence reveals that this is typical of NASA parawings. To account for the large canopy slackness of these wings when using lifting-line techniques, twist and camber distributions are treated as an aerodynamic variation in angle of attack across the wing span. In view of this, the Prandtl lifting-line theory was applied to the wide range of parawings with small diam frame members reported in Ref. 3. With regard to drag properties, it should be pointed out that wing theory does not predict profile or friction drag. These components of drag were predicted by application of available methods in the literature at various stations across the span and obtaining an integrated average for the entire wing.

Canopy Geometry

The use of rigid wing theory requires an appropriate mathematical model to describe the parawing canopy surface. The assumption was made that each panel shape is conical and parabolic. The geometry of the canopy in the $X'Y'$ coordinate system, described in Fig. 2, is given by

$$Z = [\Delta/C_R X' \cos(\epsilon/2)][X'^2 - Y'^2 \cot^2(\epsilon/2)] \quad (1)$$

To determine Δ/C_R in these equations it is assumed that the trailing edge is of the parabolic form and, when the boundary conditions are applied, is described by the equation

$$Z_t = \Delta(1 - 4Y_t'^2/l^2) \quad (2)$$

The use of Eq. (1) to describe the parawing surface does not account for the geometry of the frame members nor any canopy distortions that may occur at low angles of attack. However, it does present a model for high slackness canopies which is impossible with a conical model.

The geometric twist distribution (variation in angle of attack of local chord) may also be determined from Eq. (1). The angle of attack of the local chord relative to the root

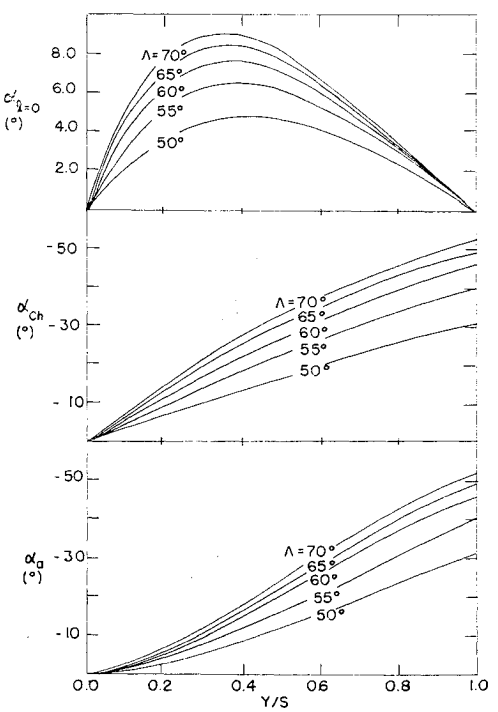

Fig. 3 Twist distribution of the basic $\Lambda_0 = 45°$ parawings.

chord, or keel (α_{Ch} in Fig. 2) is defined

$$\alpha_{Ch} = \tan^{-1}(Z_t/C) \tag{3}$$

The geometric twist distribution is presented in Fig. 3. The results indicate that for a section near the wing tip, the local chord is at large negative angles of attack with respect to the root chord. The value of α_{Ch} at the wing tip is a limiting value, as both the projected chord and the trailing edge ordinate become zero at the tip.

The local angle of zero lift also varies across the wing span because the local camber is not constant. To determine the local angle of zero lift due to camber, thin airfoil theory was employed. In order to use the results of thin airfoil theory in determining the section angle of zero lift, a translation and rotation of the coordinates used in Eq. (1) was necessary. This manipulation was performed in order to place the center of the coordinate system at the leading edge of each local chord such that the X'' axis lay along the local chord and the Z'' axis was perpendicular to the local chord with the Y' axis remaining unchanged, as indicated in Fig. 2.

Results for the camber distribution for the basic 45° parawing with leading edge sweep angles of 50°, 60°, and 70° are presented in Fig. 4. For a given parawing the maximum camber occurs in the neighborhood of $0.4S$. The actual location of maximum camber proceeds from approximately $0.3Ch$ at $0.2S$ to $0.5Ch$ at $0.8S$. The effect of increasing the canopy slackness is to correspondingly increase the maximum camber across the span.

The computed section angle of zero lift is presented in Fig. 3. The results indicate that increasing the sweep angle increases the angle of zero lift at a given spanwise position. The angle of attack for any section relative to the root chord can now be obtained from the relation

$$\alpha_a = \alpha_{Ch} + \alpha_{l=0} \tag{4}$$

The absolute angles of attack are also given in Fig. 3.

Analysis Based on Finite Wing Theory

The fundamental equation of Prandtl's finite wing theory[24] is

$$\alpha = \alpha_o + \alpha_i \tag{5}$$

where α_o is the angle of attack for the two-dimensional wing of infinite span and α_i is the additional angle of attack produced by the trailing vorticies of the finite wing. The sum of these two angles of attack at any wing section must equal the geometric angle of attack α at that station. The induced angle of attack at any position on the span can be written in terms of the downwash velocity caused by the trailing vortex. The two-dimensional angle of attack is

$$\alpha_o = C_l/a_o \tag{6}$$

where a_o is the two-dimensional lift curve slope. The two-dimensional lift curve slope was assumed to be constant and equal to 5.15/rad as given[25] for the Farman airfoil, which is somewhat similar to parawing sections. Upon substitution of these equations together with the series for circulation into Eq. (5), the geometric angle of attack becomes

$$\alpha(\theta) = \frac{1}{\mu \sin\theta} \sum_{n=1}^{\infty} A_n \sin n\theta(\mu n + \sin\theta) \tag{7}$$

where

$$\mu = a_o(\theta)Ch(\theta)/8S$$

and, in general, the parameters α, a_o, and Ch can all vary with θ across the span. Equation (7) is valid at any value of θ and the number of coefficients A_n is determined by the number of locations on the wing where this relation is satisfied. Introducing the parawing geometry into the basic

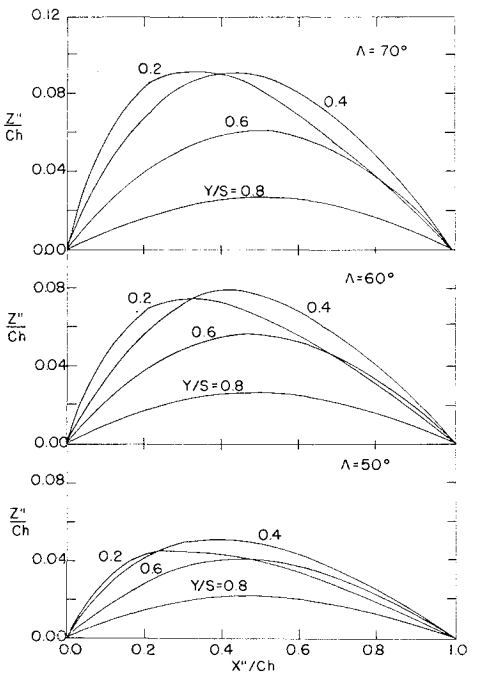

Fig. 4 Camber distribution of the basic $\Lambda_0 = 45°$ parawings.

equation of finite wing theory at a given number of spanwise stations and determining the coefficients A_n in the circulation series allows the parawing lift and induced drag coefficients to be obtained.

To determine the series coefficients for a given paraglider at a given angle of attack, the various parameters must be expressed in terms of paraglider geometry. The geometric angle of attack is

$$\alpha = \alpha_K + \alpha_a \tag{8}$$

where α_K is the angle of attack of the keel member or root chord and α_a is defined in Eq. (4).

Equation (7) is then solved at a finite number of positions on the semispan to evaluate the A_n coefficients. Since the wing is symmetrical about its root chord only the odd coefficients remain in the sine series. Other investigators have found that the successive coefficients $A_1, A_3, A_5, \ldots$ decrease rapidly in size so that satisfactory accuracy is obtained by choosing only four points to satisfy Eq. (7). However, since the parawing sections change drastically from root to tip, 8 positions on the semispan were chosen to satisfy Eq. (7). The values of θ corresponding to the 8 positions are $\pi/16$ through $\pi/2$ in increments of $\pi/16$. This corresponds to Y coordinates at 0.981, 0.925, 0.832, 0.707, 0.568, 0.383, 0.192, and 0.0 of the semispan. This distribution places emphasis on the stations near the tip where the wing sections and the circulation pattern change rapidly. Rearranging Eq. (7) with the proper substitutions, one obtains

$$[\alpha_K + \alpha_a(\theta)] \sin\theta = \sum_{n=1,3,5\ldots}^{\infty} A_n \sin n\theta \left(n + \frac{\sin\theta}{\mu}\right) \tag{9}$$

The following procedure was used to solve these equations and, thus, determine the lift and drag properties for a given parawing geometry. First the (Δ/C_R) parameter was determined for the given employed and basic sweep angles. Second the keel angle of attack was set at some arbitrary value. Next the coefficients of Eq. (9) were determined for each θ_i from $\pi/16$ to $\pi/2$. The resulting 8×8 matrix was solved numerically using Gaussian elimination with partial pivoting followed by backward substitution. The solution to this matrix produced the first eight coefficients in the circulation series.

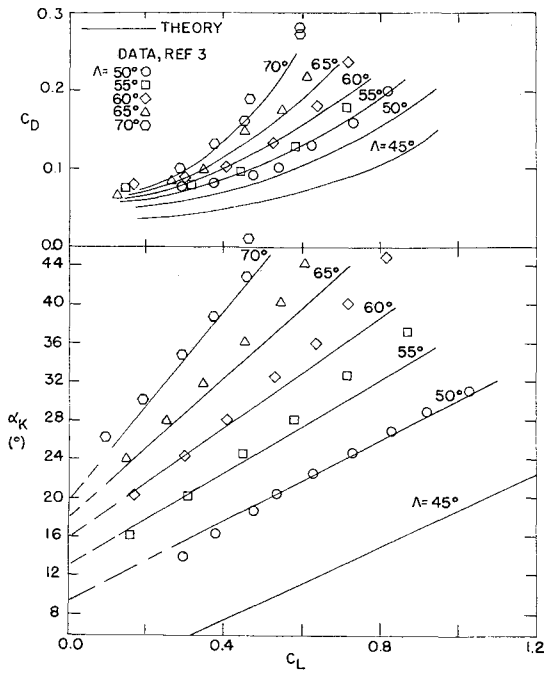

Fig. 5 Comparison of theoretical and experimental lift and drag coefficients of the basic $\Lambda_0 = 45°$ parawings.

Because the induced drag does not account for the total wing drag, the profile drag must also be predicted. This type of drag can be attributed to skin-friction drag and the pressure drag that occurs along the rear of the cambered sections. The total wing drag for parawings must also include the effect of the leading edge drag of the frame members. Therefore,

$$C_D = C_{D_i} + C_{D_{le}} + C_{D_o} \tag{10}$$

The induced drag coefficient after integration becomes

$$C_{D_i} = \frac{C_L^2}{\pi AR} \sum_{n=1}^{\infty} \frac{nA_n^2}{A_1} \tag{11}$$

The skin-friction drag was estimated[19] as that for the turbulent flow at a Reynolds number R_c based on the mean aerodynamic chord. The pressure drag associated with the adverse pressure gradient along the afterbody of streamline airfoil sections was included.[26] This pressure or separation drag was assumed to be proportional to the friction drag. For a section with thickness (t/Ch) the viscous drag (friction plus pressure) at zero lift is

$$C_{d_{o_{l=0}}} = \frac{0.148}{R_c^{0.2}} \frac{\sin\epsilon_o}{\sin\epsilon}\left[1 + 2\left(\frac{t}{Ch}\right) + 60\left(\frac{t}{Ch}\right)^4\right] \tag{12a}$$

for sections where the maximum thickness occurs at 30% of the chord, and

$$C_{d_{o_{l=0}}} = \frac{0.148}{R_c^{0.2}} \frac{\sin\epsilon_o}{\sin\epsilon}\left[1 + 1.2\left(\frac{t}{Ch}\right) + 70\left(\frac{t}{Ch}\right)^4\right] \tag{12b}$$

for sections where the maximum thickness is located at 40 to 50% of the chord.

Equations (12a) and (12b) permit the determination of profile drag coefficient at each section on the parawing span. However, these values of profile drag are valid only when the local lift coefficient C_l is zero. As the wing angle of attack is increased, the lift coefficient rises and the boundary layer along the wing surface is altered. The effect is to increase the profile drag. This has been estimated[27] as

$$C_{d_o} = C_{d_{o_{l=0}}} + 0.0093C_l^{3.2} \tag{13}$$

The local lift coefficient in Eq. (13) can be determined in terms of the circulation series

$$C_l = 8S \sum_{n=1}^{\infty} A_n \frac{\sin n\theta}{Ch} \tag{14}$$

Because the camber and the local lift coefficients vary across the parawing span, the profile drag is different at each spanwise station. To determine the wing profile drag an integrated average of the local profile drag coefficients was taken across the wing semispan since the parawing is symmetrical about its root chord. This wing profile drag is defined as

$$C_{D_o} = \int_0^S C_d(Y)dY \Big/ \int_0^S dY \tag{15}$$

The drag of the leading edge members was estimated in Ref. 19 by using simple sweep theory as

$$C_{D_{le}} = 2(d/l_{le})C_{D_c} \sin^2\epsilon \tag{16}$$

where C_{D_c} is a cross flow drag coefficient based on canopy attachment. Thus, the addition of Eqs. (11), (15), and (16) yields the total parawing drag coefficient.

Results and Discussion

The theoretical analysis was applied to the basic 35°, 45°, and 55° small-diameter leading edge parawings tested in Ref. 3 to provide a basis of comparison between the theoretical and experimental results. Only the theoretical results for

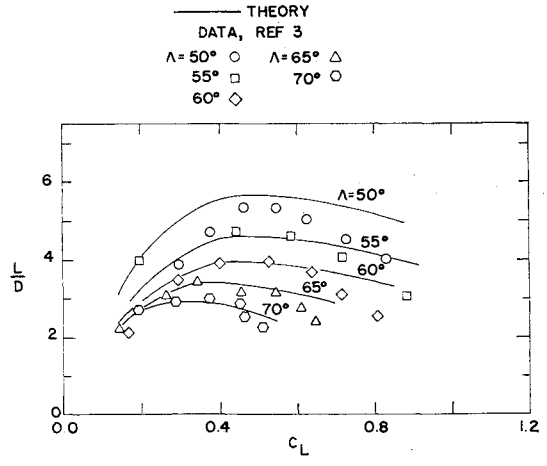

Fig. 6 Comparison of experimental and theoretical lift-to-drag ratios for basic $\Lambda_0 = 45°$ parawing.

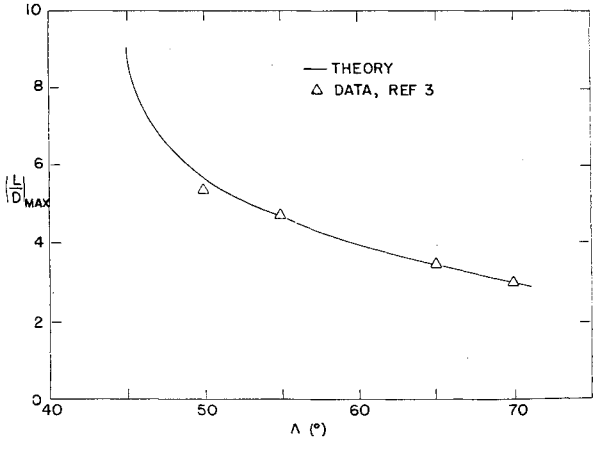

Fig. 7 $(L/D)_{max}$ as a function of sweep angle for the basic $\Lambda_0 = 45°$ parawings.

the $\Lambda_0 = 45°$ parawings will be presented as they are typical of the results. The other parawings are compared in Ref. 23.

The parawing lift and drag characteristics are presented in Fig. 5. The limiting value of the flat planform condition is given. The theoretical results are compared with experimental data[3] at the various sweep angles only at angles of attack within the linear lift range of the wing. The predicted lift is in good agreement with the experimental data.

The parawing drag characteristics are also given in Fig. 5. The theoretical drag curves are in satisfactory agreement with the experimental data. It is also observed that the theoretical drag is in better agreement with the data at low angles of attack, but the total wing drag is slightly underestimated at high lift coefficients especially for the low slackness wings. This rise in wing drag at high lift may be attributed to an increase in the viscous or profile drag due to changes in the boundary layer and the approach of separated flow.

The lift-to-drag ratio for the various sweep planforms is given in Fig. 6. The agreement between experiment and theory is reasonable (especially when one considers the scatter in the literature results) for all configurations. The maximum L/D ratio is presented as a function of the leading-edge sweep-angle in Fig. 7, where good agreement is observed between the theory and the experimental data. The largest $(L/D)_{\max}$ predicted by theory for a given basic planform is that for the flat-planform configuration. The results indicate that the change in $(L/D)_{\max}$ with sweep angle is most pronounced near the flat-planform condition.

The spanwise loading is determined from the variation in the local lift coefficient C_l across the span. This lift coefficient, as defined by Eq. (14), is indeterminant at the wing tip because both the circulation and the local chord become zero. A loading function defined as C_lCh and normalized with respect to the wing semispan S is presented in Fig. 8a for a keel angle of attack of zero degrees. Although the parawings will not operate at $\alpha_K = 0°$, this load distribution was used as a reference point. The loading at any other keel angle

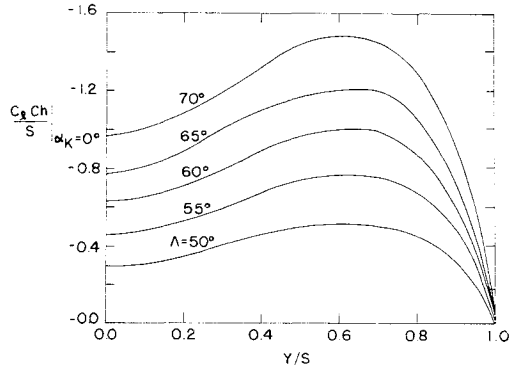

a) $\alpha_K = 0°$

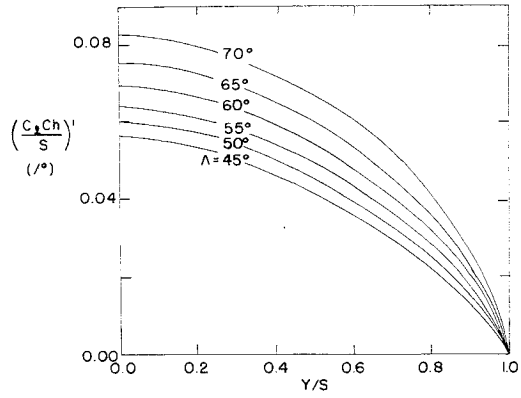

b) Spanwise loading slope

Fig. 8 Spanwise loading for the basic $\Lambda_0 = 45°$ parawings.

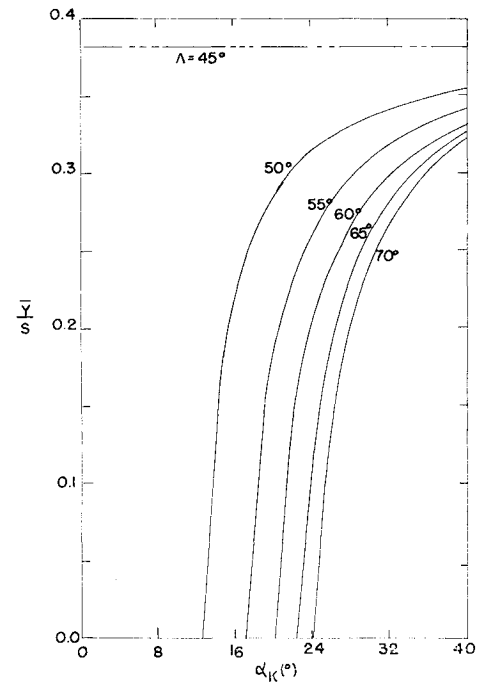

Fig. 9 Spanwise center of pressure as a function of the keel angle of attack.

of attack can be determined from the relation

$$(C_lCh/S)|_{\alpha_K} = (C_lCh/S)'\alpha_K + (C_lCh/S)|_{\alpha_K=0} \quad (17)$$

where $(C_lCh/S)'$ is the change in the loading function with respect to keel angle of attack. Since the local lift curves are also linear, this loading lift curve slope along with the reference distribution allows the spanwise loading to be calculated at any keel angle of attack. The loading lift curve slopes across the semispan are presented in Fig. 8b. The load distribution as determined from Eq. (17) for a keel angle of attack within the wing operating range reveals a loss of loading near the wing tips.

The spanwise center of pressure is given by the relation

$$\bar{Y}/S = \int_0^S Yl(Y)dY/S \int_0^S l(Y)dY \quad (18)$$

and is presented as a function of the keel angle-of-attack in Fig. 9. The center of pressure is near the keel at low keel angles of attack, but at higher angles of attack, the center of pressure moves toward the wing tip and approaches the limiting value of the no-twist flat-planform configuration. The limiting flat-planform value, which does not change with angle of attack since all sections are at the same absolute angle of attack, compares favorably with the results of Ref. 28 for flat swept wings of similar planforms. The trend in center of pressure location for the twisted wings is expected because, at low keel angles of attack, the wing tips are unloaded and the center of the spanwise pressure distribution is near the keel. However, as the keel angle of attack is increased, the tip sections become loaded and the center of pressure location is shifted toward the wing tip. Also, at a given keel angle of attack, the parawings with the largest canopy slackness (the greatest sweep from the flat planform condition) have their center of pressures nearest the keel. This trend in center of pressure location at a given keel angle of attack is also expected because the higher slackness canopies have less loading in the vicinity of the wing tips. These center of pressure locations are valid over the entire angle of attack range below separation for rigid wings. However, the results will be valid for flexible parawings only within the range of linear lift and will not apply below the flutter boundary nor above separation.

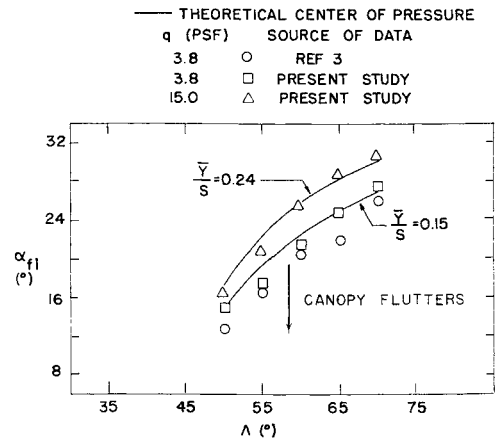

Fig. 10 Comparison of experimental and theoretical flutter boundary for the basic $\Lambda_0 = 45°$ parawings.

With regard to flutter boundary, the center of pressure data may be used to determine the keel angle of attack where flutter occurs. The flutter condition is caused by the canopy distortion which results from the wing tips becoming unloaded at low angles of attack. An examination of the center of pressures at low angles of attack reveals the following results. When the spanwise center of pressure reaches a certain position on the wing semispan, the wing tips experience such a loss in loading that canopy flutter is induced. Based on the present experimental data this position is at 15% of the semispan for a freestream dynamic pressure of 3.8 psf. Using this criterion to determine the flutter boundary at this dynamic pressure, the keel angle of attack at $\bar{Y}/S = 0.15$ is presented as a function of wing-sweep-angle in Fig. 10. The experimental results of the present investigation and those of Ref. 3 are compared with the resulting curve. The over-all agreement between the experimental data and the theoretical curve is good and indicate that the position of the center of pressure is an important parameter for determining the flutter condition. As previously pointed out, the flutter condition is a function of freestream dynamic pressure but the initial condition of canopy distortion is not. The flutter condition and canopy distortion occur simultaneously at high dynamic pressures. In order to estimate this latter point theoretically, and thus determine a safe operating range for all parawings, results of the present experimental program, for the initial condition of canopy flutter at $q_\infty = 15.0$ psf, were examined to determine the position of the center of pressure when flutter occurs. The center of pressure location based on the results of this investigation is $\bar{Y}/S = 0.24$ and the keel angle of attacks corresponding to this center of pressure are given in Fig. 10. They therefore represent the lowest keel angle of attack for safe parawing operation.

Concluding Remarks

A theoretical analysis supplemented with an experimental program has been presented for the determination of the lift and drag properties of NASA-type parawings. The experimental program was conducted to aid the theoretical analysis as well as to obtain lift and drag data on a unique series of models. The theoretical analysis enables one to determine the wing lift, induced drag, total drag, spanwise loading and center of pressure for a wide range of both high and low slackness parawings. Also, a technique based on the center of pressure results has been presented to determine the parawing angle of attack where trailing edge flutter occurs. This theoretical analysis has been applied to a large number of parawing configurations for which experimental data are available. A comparison of theory and experiment indicates that the theory yields a realistic prediction of parawing lift and drag characteristics within the linear lift range of the wing. The theoretical analysis also gives a good estimate of maximum lift-to-drag ratio and the center of pressure results can be used to give a useful estimate of trailing edge flutter.

It is significant that the present theoretical results exhibit considerable agreement with the experimental measurements of parawing lift and drag properties and therefore support the present approach based on finite wing theory. This correlation of experiment and theory indicates that, even though the theoretical approach was based on a vortex system which was confined to the plane of the parawing frame, by treating the twist distribution as a variation in the absolute angle of attack and by using the actual chord length at each station on the span, an adequate prediction of lift and drag is obtained even for high slackness parawings.

References

[1] Rogallo, F. M. et al., "Preliminary Investigation of a Paraglider," TN D-443, 1960, NASA.

[2] Polhamus, E. C. and Naeseth, R. L., "Experimental and Theoretical Studies of the Effects of Camber and Twist on the Aerodynamic Characteristics of Parawings having Nominal Aspect Ratios of 3 and 6," TN D-972, 1963, NASA.

[3] Naeseth, R. L. and Gainer, T. G., "Low-Speed Investigation of the Effects of Wing Sweep on the Aerodynamic Characteristics of Parawings having Equal-Length Leading Edges and Keel," TN D-1957, 1963, NASA.

[4] Croom, D. R., Naeseth, R. L., and Sleeman, W. C., Jr., "Effects of Canopy Shape on Low-Speed Aerodynamic Characteristics of a 55° Swept Parawing with Large-Diameter Leading Edges," TD D-2551, 1964, NASA.

[5] Croom, D. R. and Fournier, P. G., "Low-Subsonic Wind-Tunnel and Free-Flight Drop-Test Investigation of a Paraglider Configuration having Large Tapered Leading Edges and Keel," TN D-3442, 1966, NASA.

[6] Bugg, F. M., "Effects of Aspect Ratio and Canopy Shape on Low-Speed Aerodynamic Characteristics of 50.0° Swept Parawings," TN D-2922, 1965, NASA.

[7] Taylor, R. T., "Wind-Tunnel Investigation of Paraglider Models at Supersonic Speeds," TN D-985, 1961, NASA.

[8] Wornom, D. E. and Taylor, R. T., "Aerodynamic Characteristics of a Flexible-Canopy Paraglider Model at a Mach Number of 4.5 for Angles of Attack to 360° and Sideslip Angles from 0° to 90°," TN D-1776, 1963, NASA.

[9] Penland, J. A., "A Study of the Aerodynamic Characteristics of a Fixed Geometry Paraglider Configuration and Three Canopies with Simulated Variable Canopy Inflation at a Mach Number of 6.6," TN D-1022, 1962, NASA.

[10] Fournier, P. G. and Bell, B. A., "Low Subsonic Pressure Distributions on Three Rigid Wings Simulating Paragliders with Varied Canopy Curvature and Leading-Edge Sweep," TN D-983, 1961, NASA.

[11] Fournier, P. G., "Pressure Distributions on Three Rigid Wings Simulating Parawings with Varied Canopy Curvature and Leading-Edge Sweep at Mach Numbers from 2.29 to 4.65," TN D-1618, 1963, NASA.

[12] Fournier, P. G. and Bell, B. A., "Transonic Pressure Distributions on Three Rigid Wings Simulating Paragliders with Varied Canopy Curvature and Leading-Edge Sweep," TN D-1009, 1962, NASA.

[13] Pankhurst, R. C., "A Method for the Rapid Evaluation of Glauert's Expressions for the Angle of Zero Lift and the Moment at Zero Lift," R and M 1914, 1944, British Aeronautical Research Council.

[14] Weissinger, J., "The Lift Distribution of Swept-Back Wings," TM 1120, 1947, NACA.

[15] Nielsen, J. N., Kriebel, A. R., and Goodwin, F. K., "Theoretical Aerodynamics of Flexible Wings at Low Speeds, I-One-Lobed Parawings," Rept. 84, 1963, Vidya.

[16] Nielsen, J. N., Barakat, R., Goodwin, F. K., and Rudin, M., "Theoretical Aerodynamics of Flexible Wings at Low Speeds, II—Two-Lobed Parawings," Rept. 133, May 1964, Vidya.

[17] Kriebel, A. R. and Nielsen, J. N., "Theoretical Aerodynamics of Flexible Wings at Low Speeds, III—Approximate Results for Wings of Large Aspect Ratio," Rept. 146, July 1964, Vidya.

[18] Burnell, J. A. and Nielsen, J. N., "Theoretical Aerodynamics

of Flexible Wings at Low Speeds, IV—Experimental Program and Comparison with Theory," Rept. 172, Feb. 1965, Vidya.

[19] Nielsen, J. N. and Burnell, J. A., "Theoretical Aerodynamics of Flexible Wings at Low Speeds, V—Engineering Method for Estimating Parawing Performance," Rept. 209, Dec. 1965, Vidya.

[20] Nielsen, J. N., "Theory of Flexible Aerodynamic Surfaces," *Journal of Applied Mechanics*, Vol. 30, Ser. E, No. 3, Sept. 1963, pp. 435–442.

[21] Mendenhall, M. R., Spangler, S. B., and Nielsen, J. N., "Review of Methods for Predicting the Aerodynamic Characteristics of Parawings," AIAA Paper 68-10, New York, 1968.

[22] Mendenhall, M. R., Spangler, S. B., and Nielsen, J. N., "Investigation of Methods for Predicting the Aerodynamic Characteristics of Two-Lobed Parawings," CR-1166, 1968, NASA.

[23] Bass, R. L., III and Bertin, J. J., "An Experimental and Theoretical Investigation of the Lift and Drag Characteristics of Flexible Parawings at Low Subsonic Speeds," Aerospace Engineering Research Rept. 68003, July 1968, Univ. of Texas at Austin.

[24] Pope, A. W., *Basic Wing and Airfoil Theory*, Wiley, New York, 1954.

[25] Von Mises, R., *Theory of Flight*, McGraw-Hill, New York, 1945.

[26] Hoerner, S. F., *Fluid Dynamic Drag*, published by the author, Midland Park, N.J., 1965.

[27] Higgins, J. H., "The Prediction of Airfoil Characteristics," TR 312, 1929, NACA.

[28] Diederich, F. W. and Zlotnik, M., "Calculated Spanwise Lift Distributions and Aerodynamic Influence Coefficients for Swept Wings in Subsonic Flow," TN 3476, Oct. 1955, NACA.

MARCH-APRIL 1970 J. AIRCRAFT VOL. 7, NO. 2

Use of Coles' Universal Wake Function for Compressible Turbulent Boundary Layers

DOUGLAS C. MATHEWS* AND MORRIS E. CHILDS†
University of Washington, Seattle, Wash.

AND

GERALD C. PAYNTER‡
The Boeing Company, Seattle, Wash.

A two-parameter profile representation based on the law-of-the-wake and the law-of-the-wall is proposed for isoenergetic compressible turbulent boundary layers. The method of least squares was used to fit the proposed profile to experimental boundary-layer velocity profiles for a variety of flows including a normal shock induced separation, an oblique shock reflection and a flat-plate flow. Results indicate that for cases in which there is a significant departure of the boundary layer from flat-plate flow the proposed "wall-wake" profile provides a substantial improvement over the power-law representation of the velocity distribution. For both the normal shock induced separation and the oblique shock reflection, the proposed profile provided a good representation of the actual flow in the redeveloping region downstream of the interaction, indicating that the wall-wake representation should be useful in integral analysis of such flows. For all cases considered the two parameters of the profile, the boundary-layer thickness and the skin friction were found to be physically realistic.

Nomenclature

A = function of M and wall temperature, $\{[(\gamma - 1)/2] M_e^2/(T_w/T_e)\}^{1/2}$
B = function of M and wall temperature, $\{(1 + [(\gamma - 1)/2] M_e^2)/(T_w/T_e)\} - 1$
C = constant in law of the wall (usually 5.1)
C_f = skin-friction coefficient
K = constant in law of the wall (usually 0.4)
M = Mach number
Re_δ = Reynolds number based on δ
u = velocity in streamwise direction
u^* = Van Driest's generalized velocity, Eq. (6)
u_τ = friction velocity $(\tau_w/\rho_w)^{1/2}$
W = Coles' tabulated universal wake function
y = coordinate normal to wall
γ = ratio of specific heats
δ = boundary-layer thickness
μ = viscosity
ν = kinematic viscosity
π = coefficient of wake function
ρ = density
σ = $[(\gamma - 1)/2] M_e^2/\{1 + [(\gamma - 1)/2] M_e^2\}$
τ = shear stress

Subscripts

e = conditions at the edge of the boundary layer
w = conditions at the wall

Received June 2, 1969; revision received October 15, 1969. The results reported here evolved from informal discussions among the authors on studies which they were conducting of shock wave boundary-layer interactions. The portion of the work which was conducted at the University of Washington was supported by NASA Grant NGR-48-002-047, under administration of the Airbreathing Propulsion Branch, Ames Research Center.

* Graduate Student in Mechanical Engineering, University of Washington, Seattle, Wash.; presently, Assistant Project Engineer, Pratt & Whitney Aircraft, East Hartford, Conn.

† Professor, Mechanical Engineering Department, University of Washington, Seattle, Wash. Member AIAA.

‡ Research Specialist, Commercial Airplane Division, The Boeing Company, Seattle, Wash. Member AIAA.

1. Introduction

FOR incompressible boundary layers, either with or without pressure gradient, Coles' Universal Wake Function,[1] when combined with the "law of the wall," provides a good representation of turbulent boundary-layer velocity profiles.